Published in final edited form as:
*Heart Rhythm*. 2011 May ; 8(5): 752–759. doi:10.1016/j.hrthm.2010.12.034.

# Mapping of Cardiac Electrical Activation with Electromechanical Wave Imaging: An in silico-in vivo Reciprocity Study

**Jean Provost, MS**[1], **Viatcheslav Gurev, PhD**[2], **Natalia Trayanova, PhD, FHRS**[*,2], and **Elisa E. Konofagou, PhD**[*,1,3]

[1]Department of Biomedical Engineering, Columbia University, New York, NY, USA

[2]Department of Biomedical Engineering and Institute for Computational Medicine, Johns Hopkins University, Baltimore, MD, USA

[3]Department of Radiology, Columbia University, New York, NY, USA

## Abstract

**Background—**Electromechanical Wave Imaging (EWI) is an entirely non-invasive, ultrasound-based imaging method capable of mapping the electromechanical activation sequence of the ventricles *in vivo*. Given the broad accessibility of ultrasound scanners in the clinic, the application of EWI could constitute a flexible surrogate for the 3D electrical activation.

**Objective—**The purpose of this report is to reproduce the electromechanical wave (EW) using an anatomically-realistic electromechanical model, and establish the capability of EWI to map the electrical activation sequence *in vivo* when pacing from different locations.

**Methods—**EWI was performed in one canine during pacing from three different sites. A high-resolution dynamic model of coupled cardiac electromechanics of the canine heart was used to predict the experimentally recorded electromechanical wave. The simulated 3D electrical activation sequence was then compared with the experimental EW.

**Results—**The electrical activation sequence and the EW were highly correlated for all pacing sites. The relationship between the electrical activation and the EW onset was found to be linear with a slope of 1.01 to 1.17 for different pacing schemes and imaging angles.

**Conclusions—**The accurate reproduction of the EW in simulations indicates that the model framework is capable of accurately representing the cardiac electromechanics and thus testing new hypotheses. The one-to-one correspondence between the electrical activation sequence and the EW indicates that EWI could be used to map the cardiac electrical activity. This opens the door for further exploration of the technique in assisting in the early detection, diagnosis and treatment monitoring of rhythm dysfunction.



Correspondence to: Dr. Natalia Trayanova, 3400 N. Charles St., CSEB 216, Baltimore, MD, 21218, ntrayanova@jhu.edu, Phone: 410-516-4375, Fax: 410-516-5294.
*equal contribution senior authors

**Keywords**

Electrical activation sequence; Electromechanical wave imaging; Electromechanical model of the heart; High frame-rate echocardiography; Image-based computational modeling; Ventricular contraction

## Introduction

Disturbances in the electrical activation of the heart constitute a major cause of death and disability, affecting millions of people worldwide. However, no imaging method is currently capable of mapping the three-dimensional (3D) electrical activation sequence in the heart for clinical use. Currently available clinical methods are all catheter-based, and are thus limited to mapping the endocardial or epicardial activation sequence; they are also time-consuming and costly. Newly developed electrocardiographic imaging methods based on high density, body surface potential maps hold high promise for reconstruction of the 3D activation sequence in the heart[1,2] and have demonstrated clinical relevance[3,4]. However, these methods rely on either ionizing exposure, i.e., three-dimensional computed tomography, or MRI, which can be contraindicated for patients with pacemakers or stents. Even in a laboratory setting, mapping the 3D electrical activation sequence of the heart can be a daunting task[5]. Studies of transmural electrical activation usually require usage of a large number of plunge electrodes to attain sufficient resolution[6-8], or are applied to small regions of interest in vivo[9], or to small animals, e.g., the rabbit[2]. Optical imaging methods can map the activation sequence of *ex vivo* tissue on the endo- and epicardial surfaces[10-12] and transmurally [13-16].

Recently, we have developed a novel imaging technique termed Electromechanical Wave Imaging (EWI), which is an entirely non-invasive, non-ionizing, ultrasound-based imaging method capable of mapping along various echocardiographic planes *in vivo*[17] the electromechanical activation sequence, i.e., the sequence of first instants at which the muscle transitions from a relaxation to a contraction state following the electrical activation of the heart. Spatially, this electromechanical activation forms a wavefront, i.e., the EW, that follows a propagation pattern similar to the electrical activation sequence. EWI maps the EW with high accuracy, by using a frame rate up to seven times larger than that of standard echocardiography. In its essence, EWI uses cross-correlation of the radio-frequency (RF) signals to estimate the minute, electromechanically induced, inter-frame axial strains at an accuracy and spatial resolution never achieved before in a full view of the heart within a 2-3 millisecond-long time interval. Using these inter-frame axial strains, the timings at which a region in the heart transitions from a relaxing to a contracting state of the heart can be mapped.

EWI has previously been performed in mice[18], dogs[19] and humans[20]. These reports have demonstrated correlation of the EW with the pacing protocol and the conduction velocity of the electrical wave[18], and have shown that EWI can be used to determine the location of the pacing site[21] and map the presence of ischemic regions[17]. Since the only required equipment to perform EWI is a clinical ultrasound scanner[20], the application of EWI as a surrogate for the 3D electrical activation in the ventricles can be flexible and broad, at the doctor's office or point of care, to identify patients at risk, inform caregivers, or plan, monitor and assist with follow-up of therapeutic interventions such as cardiac resynchronization therapy and ablation. However, in order to exploit the full potential of EWI in the clinic, it is of paramount importance that the degree to which EWI adequately represents the pattern of 3D electrical activation in the ventricles is explicitly determined.

In order to perform such evaluation, the propagation of the EW needs to be compared to the 3D electrical activation in the ventricles, preferably in a large animal heart, such as the canine one. However, available experimental methods do not allow for simultaneous mapping of both the EW and the 3D (and in particular, the transmural) electrical activation sequence. Indeed, the spatial resolution of plunge needle recordings is insufficient for the adequate comparison with the EW sequence; moreover, since the strains associated with the EW are minute[17], the insertion of needle electrodes is likely to significantly alter the normal EW.

Due to the limitations in current experimental techniques for mapping the 3D electrical activation sequence with high spatiotemporal resolution, an anatomically-realistic modeling approach to cardiac function appears as an attractive alternative in providing the 3D electrical activation sequence in the ventricles. We developed a high-resolution dynamic model of coupled cardiac electromechanics in the rabbit heart[22] and used it to ascertain the mechanisms of spontaneously induced arrhythmias in acute regional ischemia[23]. The model was recently extended to the canine heart, where the geometry and structure of the canine heart was reconstructed from MRI and diffusion tensor (DT) MRI scans[24]. In this study, we use this novel electromechanics model of the canine heart for the first time and apply it, after optimizing it, to fully assess the utility of EWI in mapping the electrical activation sequence in the canine ventricles.

To achieve this goal, we simulate the EW in the model of the normal canine ventricles and compare the results to the *in-vivo* experimental EW in the canine. Once the match between simulated and experimental EWs is obtained and the predictive capabilities of the canine electromechanics model are established, the EW is compared to the electrical activation sequence obtained from the model, providing the desired relationship between the EW and the 3D electrical activation maps in the canine ventricles, and thus assessing the utility of EWI in mapping the electrical activation.

## Methods

### Experimental protocol

In this study, approved by the Institutional Animal Care and Use Committee of Columbia University, one male mongrel dog, of 28 kg in weight, was anesthetized with an intravenous injection of thiopental (10-17mg/kg). The animal was mechanically ventilated with a rate- and volume-regulated ventilator on a mixture of oxygen and titrated isoflurane (0.5-5.0%). Morphine (0.15mg/kg, epidural) was administered before surgery, and lidocaine (50 micrograms/kg/hr, intravenous) was used during the procedure. To maintain blood volume, 0.9% saline solution was administered intravenously at 5mL/kg/hr. Solid-state pressure transducer catheters (Millar Instruments, Houston, TX) were inserted into the left-ventricular (LV) cavity via the right carotid artery and the aorta. The chest was opened by lateral thoracotomy using electrocautery. After removal of the pericardium, three crystals of 2-mm in diameter combined with bipolar pacing electrodes were sutured onto the epicardium at the following locations: 1) basal region of the lateral wall (LVb), 2) LV apex (LVa) and 3) RV apex (RVa) and used to pace the ventricles.

### Electromechanical Wave Imaging

An Ultrasonix RP (Ultrasonix Medical Corp., Burnaby, BC, Canada) system with a 3.3MHz phased array was used to acquire RF frames at 370 frames/s (fps) using an automated composite technique[20] (Figure 1A). Briefly, this method involves increasing the frame rate by dividing the image into partially overlapping sectors corresponding to separate cardiac cycles. The probe was attached to a stabilizer (Medtronic Corp., Minneapolis, MN) and the

respirator was interrupted for 6 to 20s during ultrasound acquisition. The axial inter-frame displacements were obtained with a RF-based cross-correlation method (window size: 4.6mm, 80% overlap) and the full-view image was then reconstructed using the motion-matching technique[17]. Briefly, this method does not rely on the ECG and consists of comparing the inter-frame displacements measured in the overlapping region of two sectors to synchronize each set of neighboring sectors, allowing the reconstruction of the full-view of the heart, i.e., the EWI ciné-loop (Figure 1B).

The axial inter-frame strains were mapped in Eulerian coordinates, estimated using a least-squares estimator[25] (kernel of 6.75 mm) and overlayed on the B-mode ultrasound images. The myocardium was segmented using an automated contour tracking technique[26]. To generate the isochrones, zero-crossing points were identified in three regions where the ultrasound beam was best aligned with either the radial or the longitudinal direction of the lateral, septal and RV walls. Time delays between these regions and the nearest neighboring pixels were then obtained via normalized cross-correlation. The procedure was repeated using these neighboring pixels until the time of electromechanical activation was mapped throughout the entire echocardiographic view.

### Electromechanical model of the canine ventricles

The 3D electromechanical model of the canine ventricles has been described previously[24]. Briefly, the electromechanical model of the normal canine heart was composed of two main components, an electrical component and a mechanics component (Figure 1D). The components represented two coupled finite-element models, both based on canine ventricular geometry and structure reconstructed from *ex-vivo* cardiac MR and DTMR imaging datasets. Both the electrical and the mechanical component were biophysically-detailed, incorporating canine specific ionic and myofilament models, as described in our previous publication[24]. The mechanical and electrical components were coupled weakly to minimize computations. Finally, the electromechanical model was coupled to a model of the circulatory system representing the systemic and pulmonary circulations[24]. For the present application of the canine electromechanics model, the circulatory system model was modified to simulate backward flow from the LV to the atrium in the normal canine heart[27], by delaying mitral valve closing for 100 ms after the pacing stimuli and by increasing the mitral valve resistance by a factor of 30.

The computational mesh for the electrical component of the model consisted of linear mixed-type finite elements (1637744 elements and ~1 million nodes). The mechanics mesh was composed of non-linear, hexahedral, Hermite-based finite elements (566 elements and 1060 nodes). The generation of active stress in the myocyte was represented by active tension in the fiber and transverse to the fiber directions, calculated from the model of the cardiac myofilament. Additional details can be found in Supplemental Methods.

### Comparing the experimental EW with that in the canine electromechanics model

Consistent with the goal of this study, we compared the EW in experiment and simulation. To generate the model EW, the inter-frame axial strains resulting from an activation elicited from the same pacing site as in the experiment were calculated. For this purpose, the output of the mechanics component of the canine electromechanical model, i.e., the nodes' position, was used to obtain maps of cumulative strain over time. The simulated inter-frame strains and EWI ciné-loop (Figure 1E) were obtained by computing the temporal derivative of the cumulative strains. Simulated EWI isochrones were obtained in the same fashion as the experimental ones (Figure 1F). Since the simulations were based on a different canine heart than the one used in experiments, direct, pixel-to-pixel comparisons could not be performed. Instead, the fraction of the echocardiographic view of the ventricles, through which the EW

had propagated, was plotted as a function of time. These fractions, as obtained from experiment and simulation, were then compared directly for the three pacing schemes.

## Results

Figures 2A and 2B depict the experimental and simulated EW maps during pacing from the basal region of the lateral wall. Blue and red indicate local compression and expansion of the tissue, respectively, in the direction of the ultrasound beam (Fig 1A). In the view presented here, activation results in expansion (red) throughout the ventricles with the exception of the apical region, which undergoes local compression (blue)[17]. In both experiments and simulations, the EW emerged from the basal region of the lateral wall (Figures 2A,B). The EW then propagated towards the apex, the septum and the RV wall. Figure 2C shows representative curves of the inter-frame strains over time in the lateral and septal walls during LVb pacing for both experiments and simulations. While simulated and experimental curves are not identical, they exhibit, qualitatively, similar trends. More specifically, the inter-frame strains are negative and slowly varying before a sudden increase amounting to a few tenths of a percent. Figures 2D and 2E present the EW in experiments and simulations for pacing from the LV apex. In both experiments and simulations, the EW originated at the apex and propagated towards the base in the three walls. Figure 2F shows a comparison between simulated and experimental inter-frame strains over time at one location in the lateral wall and in the septum. In both simulations and experiments, slowly varying negative inter-frame strains are observed before a steep increase up to a maximum value of approximately 0.1%. After reaching maximum, the inter-frame strains decrease while remaining positive. Figure 2G and H shows the comparison between experimental and simulation EW when pacing from the RV apex. In this case (Figures 2G,H), the EW emerged from the RV apex and propagated towards the base and the lateral wall. Figure 2I shows a comparison between simulated and experimental inter-frame strains. In both simulations and experiments, slowly varying negative inter-frame strains are observed, followed by a sudden increase. The inter-frame strains then reach maximum at approximately 0.1%, followed by a decrease to approximately 0.025%.

Figure 3 shows the isochrones of electromechanical activation in experiments, of electromechanical activation in simulations and of electrical activation in simulations during the three pacing schemes. To further quantify the agreement between simulations and experiments, the isochronal representation of the EW was used to calculate, and then plot as a function of time, the electromechanically activated myocardial fraction in the echocardiographic view (Figure 4A). The time delay between simulations and experiments for a given fraction and a given pacing schemes was then computed. For LVb, LVa and RVa pacing, these time delays were on average (± standard deviation): 5.0 ± 4.3 ms, -2.5 ± 4.2 ms, and -4.9 ± 4.5 ms, respectively. To quantify the correlation between experiments and simulations one can also plot the simulated against the experimental fractions (Figure 4B). In such a graph, an ideal experimental reproduction would result in a slope of 1 (gray line). For LVb, LVa and RVa pacing, the regression slopes obtained through least-squares fitting were 1.17 ($R^2 = 0.98$), 0.86 ($R^2 = 0.99$) and 0.89 ($R^2 = 0.99$), respectively.

The results above indicate that the electromechanics model can reproduce the behavior of the EW during different pacing protocols. Simulations were then conducted to quantify the precision with which EWI can map electrical activation. Figure 5 shows the correlation between the simulated electrical and simulated electromechanical activations during the three pacing protocols and for the two different imaging angles commonly used clinically: parasternal (Fig. 5A) and apical (Fig. 5B) views. In all six cases, a linear relationship was obtained, with slopes ranging between 1.01 and 1.17 ($0.85 < R^2 < 0.97$) and an effective electromechanical delay (eEMD), corresponding to the intercept, varying between 20.08 and

25.22 ms. Moreover, the distance between the location of the earliest electromechanical activation site and the location of the earliest electrical activation site was computed for each pacing scheme and both views. A precision in the earliest electrical activation site localization of 4.9±3.3 mm was found.

## Discussion

The EW is a direct, tissue-level result of the cardiac excitation-contraction coupling: the depolarization of a myocyte is followed by contraction after the electromechanical delay. EWI characterizes the electromechanical activation of myofibers by mapping the inter-frame axial strains. In this study, a realistic canine cardiac electromechanics model was used to reproduce the experimentally obtained EW from three different pacing sites to better understand the relationship between EW and the electrical activation sequence in the ventricles. Current experimental methods do not allow mapping of both the transmural electrical activation sequence and the EW simultaneously and at high spatial resolution. Since the strains associated with the EW are minute, any insertion of plunge needles to map the activation sequence would inadvertently alter the normal EW. Therefore, a unique and important avenue available for comparing the EW with the electrical activation sequence is using realistic electromechanical simulations. This methodology establishes a framework that can be used to further evaluate the clinical potential of EWI as a useful tool for the diagnosis as well as treatment planning and assessment of cardiac rhythm dysfunction.

The simulation model was capable of reproducing the realistic EW characteristics observed in the canine experiments, such as spatial propagation (Fig 2), temporal shape (Fig 2), isochrones (Fig 3) and activated fraction of the ventricles (Fig 4). Since different hearts were used in simulations and experiments, a perfect reproduction of the EW observed in experiments was not expected. Even under such imperfect conditions, a good match was achieved: a regression slope varying between 0.86 and 1.17 ($R^2 > 0.98$) was found between experimental and simulated electromechanically activated myocardial fractions. The model of EW was then used to quantify the relationship between the electrical activation and the EW sequence in the normal canine heart. These were in excellent agreement for all pacing protocols and for two different imaging angles. The relationship between the electrical activation and the EW onset was found to be linear with a slope of 1.01 to 1.17 and with an intercept of 20.08 to 25.22 ms. These results are in agreement with published results, although the methods and the strain tensor components used were different: Badke et al.[28] found, using implanted beads, a slope of 1.1 with an intercept of 17 ms. Using MR tagging, Wyman et al.[29] found a slope of 1.06 with an intercept of 8.4 ms and Faris et al.[30] found a slope between 0.87 and 1.05 and an intercept between 19.4 ms and 37 ms. The slope between the electrical and electromechanical activations was closer to 1 unlike in our previous modeling results[22], which used a different definition of the electromechanical activation (based on the fiber strain) and did not include the backward flow, i.e., flow from the LV to the left atrium. The linear relationship indicates a one-to-one correspondence between the electrical activation sequences and the EW. A slope higher than one indicates that the delay between the local electrical activation and the local onset of mechanical contraction increased over time (i.e., with increasing distance away from the pacing site). In other words, EWI provided an accurate representation of the electrical activation sequence but shifted in time. While the relationship between the electrical and electromechanical activations remained linear with high correlation coefficients for all pacing schemes, EWI during LVa and RVa pacing followed more closely the electrical activation sequence than during LVb pacing. Similarly, while both apical and parasternal views provided high correlation coefficients, the parasternal view systematically provided a higher correlation coefficient between the electrical and electromechanical activations during the three different pacing schemes. These results indicate that EWI could be used for mapping of

electrical activation in normal hearts with different imaging angles and for different pacing protocols. Finally, EWI was also found capable of identifying the region of earliest electrical activation with an accuracy of approximately 5 mm.

Since the inter-frame deformations estimated and mapped in EWI are minute (<0.25% at 370 fps) and their propagation is fast (0.5-2 m/s), they are not detected with existing imaging modalities in the clinic, such as standard echocardiography or MRI. Currently, no imaging modality other than EWI can capture the electromechanics of both ventricles with an accuracy up to ten times higher than commercial B-mode speckle-tracking algorithms and at frame rates reaching 370-500 fps, i.e., imaging at 2-2.7ms intervals[20]. By comparison, MRI tagging typically provides images every 50 ms, although novel approaches based on ECG-gating over 128 heartbeats have been able to reach a resolution of 8ms[30].

The present study provided the proof-of-concept for the utility of EWI in mapping non-invasively the 3D electrical activation in the heart. This study focused on the electromechanical behavior of a normal, paced heart. In the presence of disease, the electromechanical coupling could be affected and thus could alter the capability of EWI to map the electrical activation sequence. However, since EWI is a direct method, the displacements and strains measured during the QRS complex remain accurate in regions of remodeling and can be used to identify the extent of the problem, e.g., ischemia[17]. Moreover, the RF signals acquired at very high frame rates for EWI can also be used to map standard measures at higher accuracy such as cumulative systolic strains, which can also be used to identify or confirm the presence of ischemic or infarcted regions[31].

This study presents the first application of the new MRI-based electromechanical model of the canine ventricles[24]. Previous ventricular electromechanical models[32-34] incorporated ventricular geometries and fiber architecture that were obtained from histological sections; this labor-intensive procedure resulted in the development of only three histology-based anatomical models. In contrast, obtaining MR and DTMR scans of an ex-vivo heart is a relatively fast procedure. When it is combined with our new semi-automatic procedure for model construction[24], generating a whole-heart electromechanical model becomes a high-throughput process, providing the capability to assemble electromechanical models for any species under normal or pathological conditions. The electromechanics model also incorporates a new approach to the generation of finite-element mechanics meshes and the use of tensors to describe ventricular fiber and laminar sheet architecture, as well as detailed biophysical representations of both electrical and mechanical cellular activity. This approach thus provides a biophysically-based, highly-detailed modeling framework that can be used to successfully address issues related to both disturbances in heart rhythm and the efficacy of the cardiac pump.

## Implications of the Study

In this study, the EW was reproduced accurately with the realistic cardiac electromechanics model, indicating that the model framework is capable of faithfully representing the physiology of cardiac electromechanics and that it could thus be used to test new hypotheses. Furthermore, a strongly-correlated, linear relationship was found between the electrical activation sequence and the EW onset in the normal heart, ascertaining the potential of EWI to map non-invasively the electrical activation sequence of the heart *in-vivo*. These achievements could potentially lead to the establishment of a new, noninvasive, non-ionizing, at-the-point-of-care imaging modality, capable of assisting early detection and diagnosis of rhythm disturbances, which could help to better plan, monitor and follow-up the treatment of a wide range of arrhythmias.

## Limitations

Different canines were used for EWI and the electromechanics model. Discrepancies in geometry and structure could thus have affected the correspondence between experimental and simulated images. Although EWI is applicable transthoracically[20], this study was conducted in an open-chest setting to allow the implantation of pacing electrodes. The EW and the electrical activation sequence could exhibit a different relationship in a more clinically-relevant, closed-chest setting. Finally, consistent with the goals of the study, this relationship was characterized only in the normal ventricles. Further exploration of this relationship in the presence of disease, such as infarction or ischemia, is the topic of future studies.

## Supplementary Material

Refer to Web version on PubMed Central for supplementary material.

## Acknowledgments

The authors wish to thank Wei-Ning Lee, Kana Fujikura, Edward Ciaccio, Eiichi Hyodo, Asawinee Danpinid, Aram Safarov, and Ihsaan Sebro for their help during experiments; and Heather S. Duffy, Peter Danilo, and Iryna N. Shlapakova for their advice on the experimental procedure. The authors also wish to thank Jianwen Luo and Stanley J. Okrasinski for helpful discussions.

This study was supported in part by the National Institutes of Health (R01EB006042, R21HL096094) and Wallace H. Coulter Foundation. J.P. was funded in part by the Natural Sciences and Engineering Research Council of Canada (NSERC) and by Fonds Québécois de la Recherche sur la Nature et les Technologies (FQRNT).

## References

1. Ramanathan C, Ghanem RN, Jia P, Ryu K, Rudy Y. Noninvasive electrocardiographic imaging for cardiac electrophysiology and arrhythmia. Nat Med. 2004; 10(4):422–428. [PubMed: 15034569]
2. Zhang X, Ramachandra I, Liu Z, et al. Noninvasive three-dimensional electrocardiographic imaging of ventricular activation sequence. Am J Physiol Heart Circ Physiol. 2005; 289(6):H2724–32. [PubMed: 16085677]
3. Berger T, Fischer G, Pfeifer B, et al. Single-Beat Noninvasive Imaging of Cardiac Electrophysiology of Ventricular Pre-Excitation. Journal of the American College of Cardiology. 2006; 48(10):2045–2052. [PubMed: 17112994]
4. Ghosh S, Rhee EK, Avari JN, Woodard PK, Rudy Y. Cardiac Memory in Patients With Wolff-Parkinson-White Syndrome: Noninvasive Imaging of Activation and Repolarization Before and After Catheter Ablation. Circulation. 2008; 118(9):907–915. [PubMed: 18697818]
5. Nash MP, Pullan AJ. Challenges Facing Validation of Noninvasive Electrical Imaging of the Heart. The Annals of Noninvasive Electrocardiology. 2005; 10(1):73–82.
6. Chattipakorn N, Fotuhi PC, Chattipakorn SC, Ideker RE. Three-Dimensional Mapping of Earliest Activation after Near-Threshold Ventricular Defibrillation Shocks. J Cardiovasc Electro. 2003; 14(1):65–69.
7. Durrer D, Van Dam RT, Freud GE, et al. Total Excitation of the Isolated Human Heart. Circulation. 1970; 41(6):899–912. [PubMed: 5482907]
8. Sutherland DR, Ni Q, MacLeod RS, Lux RL, Punske BB. Experimental measures of ventricular activation and synchrony. Pacing Clin Electrophysiol. 2008; 31(12):1560–1570. [PubMed: 19067808]
9. Ashikaga H, Coppola BA, Hopenfeld B, et al. Transmural Dispersion of Myofiber Mechanics: Implications for Electrical Heterogeneity In Vivo. Journal of the American College of Cardiology. 2007; 49(8):909–916. [PubMed: 17320750]

10. Kay MW, Amison PM, Rogers JM. Three-dimensional surface reconstruction and panoramic optical mapping of large hearts. IEEE Trans Biomed Eng. 2004; 51(7):1219–1229. [PubMed: 15248538]
11. Qu F, Ripplinger CM, Nikolski VP, Grimm C, Efimov IR. Three-dimensional panoramic imaging of cardiac arrhythmias in rabbit heart. J Biomed Opt. 2007; 12(4):044019. [PubMed: 17867823]
12. Ripplinger CM, Lou Q, Li W, Hadley J, Efimov IR. Panoramic imaging reveals basic mechanisms of induction and termination of ventricular tachycardia in rabbit heart with chronic infarction: implications for low-voltage cardioversion. Heart Rhythm. 2009; 6(1):87–97. [PubMed: 18996057]
13. Hooks DA, LeGrice IJ, Harvey JD, Smaill BH. Intramural multisite recording of transmembrane potential in the heart. Biophys J. 2001; 81(5):2671–2680. [PubMed: 11606280]
14. Kong W, Ideker RE, Fast VG. Transmural optical measurements of Vm dynamics during long-duration ventricular fibrillation in canine hearts. Heart Rhythm. 2009; 6(6):796–802. [PubMed: 19467507]
15. Hillman EMC, Bernus O, Pease E, Bouchard MB, Pertsov A. Depth-resolved optical imaging of transmural electrical propagation in perfused heart. Opt Express. 2007; 15(26):17827–17841. [PubMed: 18592044]
16. Baxter WT, Mironov SF, Zaitsev AV, Jalife J, Pertsov AM. Visualizing Excitation Waves inside Cardiac Muscle Using Transillumination. Biophysical Journal. 2001; 80(1):516–530. [PubMed: 11159422]
17. Provost J, Lee W, Fujikura K, Konafagou E. Electromechanical Wave Imaging of Normal and Ischemic Hearts in Vivo. IEEE Trans Med Imaging. 2010; 29(3):625–635. [PubMed: 19709966]
18. Konofagou EE, Luo J, Saluja D, et al. Noninvasive electromechanical wave imaging and conduction-relevant velocity estimation in vivo. Ultrasonics. 2010; 50(2):208–215. [PubMed: 19863987]
19. Pernot, M.; Konofagou, EE. Electromechanical imaging of the myocardium at normal and pathological states. Ultrasonics Symposium, 2005 IEEE; 2005. p. 1091-1094.
20. Wang S, Lee W, Provost J, Luo J, Konofagou EE. A composite high-frame-rate system for clinical cardiovascular imaging. Ultrasonics, Ferroelectrics and Frequency Control, IEEE Transactions on. 2008; 55(10):2221–2233.
21. Provost, J.; Gurev, V.; Trayanova, N.; Konofagou, EE. Characterization of Wave Origins in Electromechanical Wave Imaging. 2008 IEEE International Ultrasonics Symposium; Beijing, China. 2008.
22. Gurev V, Constantino J, Rice JJ, Trayanova NA. Distribution of electromechanical delay in the heart: insights from a three-dimensional electromechanical model. Biophys J. 2010; 99(3):745–754. [PubMed: 20682251]
23. Jie X, Gurev V, Trayanova N. Mechanisms of Mechanically Induced Spontaneous Arrhythmias in Acute Regional Ischemia. Circ Res. 2010; 106(1):185–192. [PubMed: 19893011]
24. Gurev, V.; Lee, T.; Constantino, J.; Arevalo, H.; Trayanova, NA. Models of cardiac electromechanics based on individual hearts imaging data : Image-based electromechanical models of the heart. Biomech Model Mechanobiol. 2010. Available at: http://www.ncbi.nlm.nih.gov/pubmed/20589408
25. Kallel F, Ophir J. A least-squares strain estimator for elastography. Ultrason Imaging. 1997; 19(3): 195–208. [PubMed: 9447668]
26. Luo J, Konofagou EE. High-frame rate, full-view myocardial elastography with automated contour tracking in murine left ventricles in vivo. Ultrasonics, Ferroelectrics and Frequency Control, IEEE Transactions on. 2008; 55(1):240–248.
27. Otsuji Y, Handschumacher MD, Schwammenthal E, et al. Insights From Three-Dimensional Echocardiography Into the Mechanism of Functional Mitral Regurgitation : Direct In Vivo Demonstration of Altered Leaflet Tethering Geometry. Circulation. 1997; 96(6):1999–2008. [PubMed: 9323092]
28. Badke FR, Boinay P, Covell JW. Effects of ventricular pacing on regional left ventricular performance in the dog. Am J Physiol Heart Circ Physiol. 1980; 238(6):H858–867.

29. Wyman BT, Hunter WC, Prinzen FW, McVeigh ER. Mapping propagation of mechanical activation in the paced heart with MRI tagging. Am J Physiol Heart Circ Physiol. 1999; 276(3):H881–891.

30. Faris OP, Evans FJ, Ennis DB, et al. Novel Technique for Cardiac Electromechanical Mapping with Magnetic Resonance Imaging Tagging and an Epicardial Electrode Sock. Ann Biomed Eng. 2003; 31(4):430–440. [PubMed: 12723684]

31. Lee, W.; Provost, J.; Fujikura, K.; Wang, J.; Konofagou, E. In vivo validation of Myocardial Elastography under graded ischemia conditions. 2010 7th IEEE ISBI Proceedings; 2010. p. 972-975.

32. Nickerson D, Smith N, Hunter P. New developments in a strongly coupled cardiac electromechanical model. Europace. 2005; 7:S118–S127.

33. Usyk TP, LeGrice IJ, McCulloch AD. Computational model of three-dimensional cardiac electromechanics. Computing and visualization in science. 2002; 4(4):249–257.

34. Vetter FJ, McCulloch AD. Three-dimensional analysis of regional cardiac function: a model of rabbit ventricular anatomy. Prog Biophys Mol Biol. 1998; 69(2-3):157–183. [PubMed: 9785937]

## Glossary of abbreviations used in the manuscript

| | |
|---|---|
| **3D** | Three-dimensional |
| **DT** | Diffusion tensor |
| **ECG** | Electrocardiogram |
| **EW** | Electromechanical Wave |
| **EWI** | Electromechanical Wave Imaging |
| **fps** | Frames per second |
| **MR** | Magnetic resonance |
| **LV** | Left-ventricle |
| **RF** | Radio-frequency |
| **RV** | Right Ventricle |
| **LVb** | Basal Region of the Lateral Wall |
| **LVa** | Apex of the Left Ventricle |
| **RVa** | Apex of the Right Ventricle |

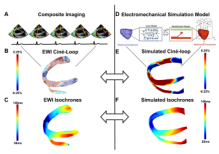

**Figure 1.**

**A:** Imaging of the heart over multiple beats. **B:** Strain-overlayed, segmented ciné-loop of the heart depicting the propagation of the EW. **C:** EWI isochrones obtained from the interpolation of manually selected zero-crossing points of hundreds of locations in the ventricle. **D:** Cardiac electromechanics model. **E:** Simulated EWI ciné-loop. **F:** Simulated EW isochrones.

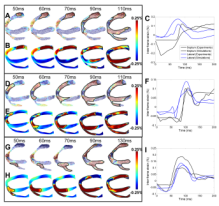

**Figure 2.**

Inter-frame strains associated with the EW during the three pacing protocols. ***LVb pacing***: **A:** Experimental EW, **B:** Simulated EW and **C:** Comparative graph over time. ***LVa pacing***: **D:** Experimental EW, **E:** Simulated EW and **F:** Comparative graph over time. ***RVa pacing*:** **G:** Experimental EW, **H:** Simulated EW and **I:** Comparative graph over time.

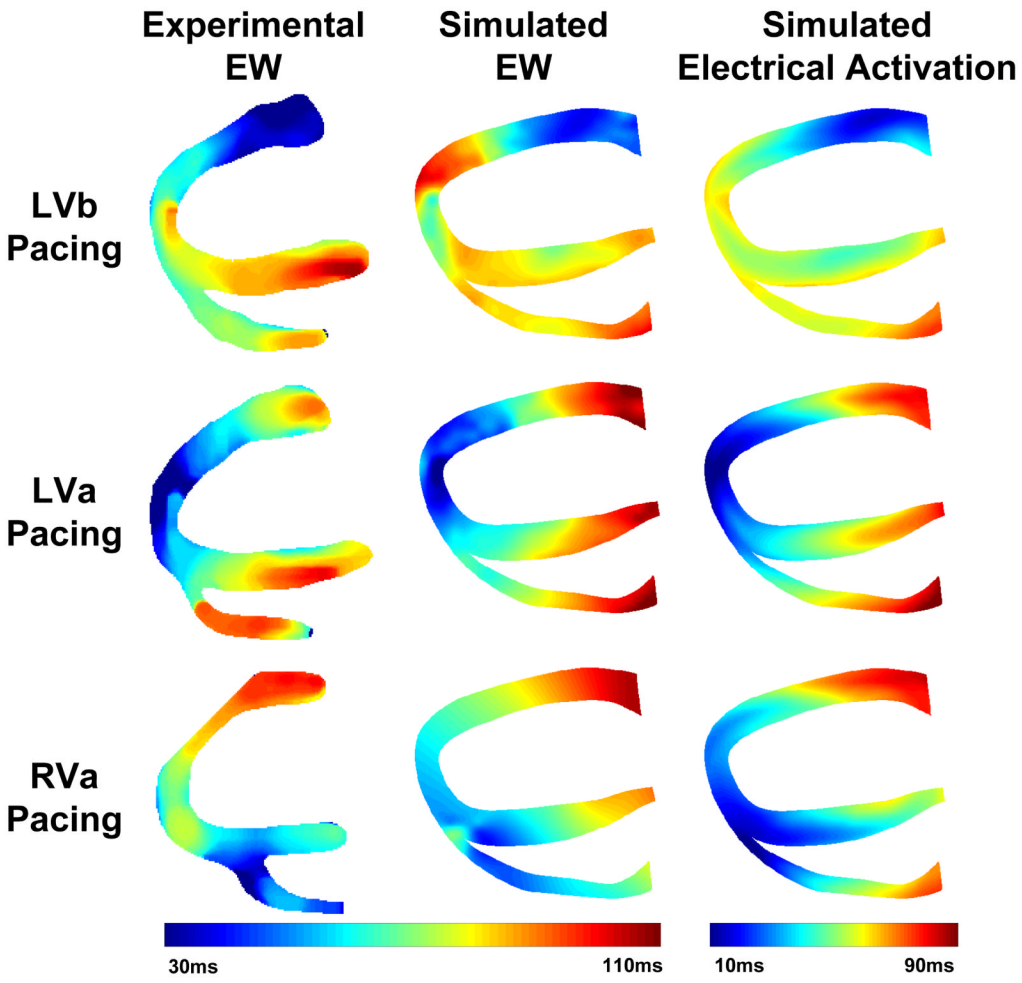


**Figure 3.**
Experimental and simulated electromechanical activation isochrones and simulated electrical activation isochrones during the three pacing protocols.

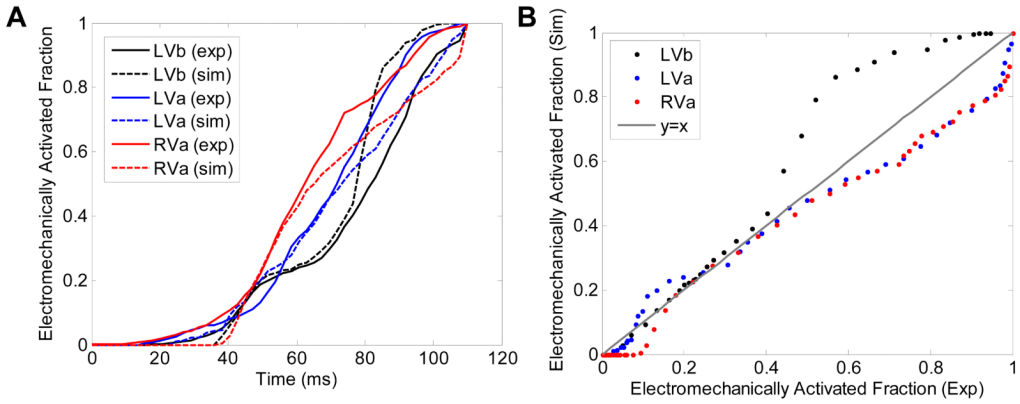


**Figure 4.**

Comparisons between experiments and simulations. **A:** Fraction of the myocardium in the echocardiographic view that underwent EW, plotted as a function of time, in experiments and simulations. **B:** Electromechanically activated myocardial fraction in the echocardiographic view in simulations, plotted as a function of the same in experiments.

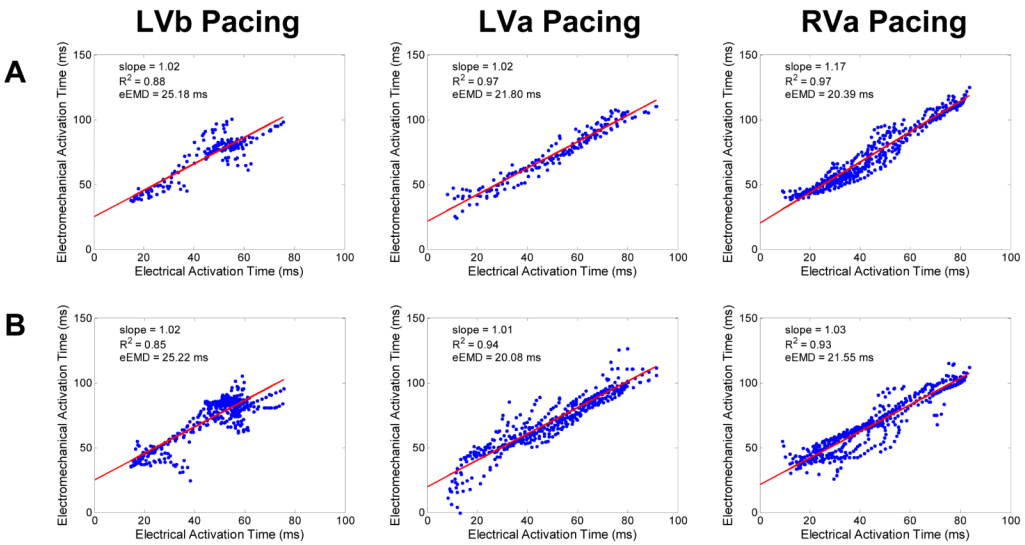


**Figure 5.**

Correlation between the electrical activation time and the electromechanical activation time when the probe is located **A:** parasternally and **B:** apically.